Journal of Materials Chemistry C

ROYAL SOCIETY OF CHEMISTRY

PAPER

View Article Online
View Journal | View Issue

Cite this: J. Mater. Chem. C, 2022, 10, 9073

UV-Visible radiation modulation abilities of photon up-converting nanocapsules integrated with an oscillatory reaction†

Giulia Quaglia, Beatrice Bartolomei, Pier Luigi Gentili and Loredana Latterini *

Radiation up-conversion through the triplet–triplet annihilation mechanism has been widely studied, mostly in solution and under de-aerated conditions. We propose oil-in-silica up-converting nanocapsules resulting in a robust solid-like material able to generate blue up-converted emission and preserve the red phosphorescence of the sensitizer under atmospheric conditions. The core phase consists of oleic acid containing the up-converting molecular pair, platinum octa-ethyl-porphyrin and 9,10-diphenyl-anthracene; the silica shell having 10–15 nm thickness acts as a protective barrier and compartmentalizes the organic molecules. The up-converted emission is measured from silica nanocapsule powder or in aqueous suspensions using an incoherent and low power density (363 μW cm^{-2}) source. The robustness of the oil-in-silica structures is tested in the acidic and oxidative solution of the oscillatory Belousov–Zhabotinsky (BZ) reaction. The BZ reaction gives rise to a modulated optical density in the UV-region. The modulated UV radiation is absorbed by the chromophores in the nanocapsules delivering periodic emissions of the capsules, which are monitored in terms of intensity amplitude and periodicity. The solidness of the nanocapsules enables employing them in a wet chemical formulation to be exposed simultaneously to the BZ-modulated UV radiation and to the steady-state Vis radiation, obtaining multiple output luminescence signals. Furthermore, the impact of simultaneous excitations empowers discussions of the intensity changes in terms of efficiencies of triplet energy transfer and establishing UC-nanostructured materials for optical communication applications.

Received 20th February 2022,
Accepted 9th May 2022

DOI: 10.1039/d2tc00709f

rsc.li/materials-c

Introduction

The development of materials and processes to convert low-energy radiation into higher-frequency light (*i.e.*, up-conversion, UC) is receiving much attention from the scientific community.[1–5] A promising and versatile mechanism to produce an apparent anti-Stokes emission[6] is the triplet–triplet annihilation (TTA)[7–9] that is based on a bimolecular process in which a dye molecule acts as a radiation antenna (or sensitizer), absorbing the low energy electromagnetic radiation and then transfers it to the emitting units. To achieve upconverted energy, the two organic molecules must have appropriate electronic energy levels and photophysical properties. The dye pair, octaethyl-porphyrin platinum(II) (PtOEP), able to act as a sensitizer (S), and 9,10-diphenylanthracene (DPA), used as an emitter (E), is nowadays a benchmark TTA-pair for green-to-blue radiation conversion, through a well-established mechanism. PtOEP successfully absorbs green light (535 nm) and, through an efficient intersystem crossing (ISC) process, populates its triplet excited state (^{3}S*). In the presence of DPA, triplet–triplet energy transfer (TTET) occurs through a Dexter-type mechanism, forming a DPA triplet excited state (^{3}E*). When high concentrations of ^{3}E* are locally formed, they can undergo exchange energy transfer processes, resulting in a triplet–triplet annihilation phenomenon (TTA). TTA leads to a DPA molecule in the singlet excited state (^{1}E*), from which fluorescence occurs, leading to the blue up-converted emission (Fig. 1).[7,10] The tight control of DPA concentration ensures to maximize the UC-emission or to detect either the blue UC-emission and the residual red phosphorescence of PtOEP.[11]

To ensure an effective triplet–triplet energy transfer (TTET), beyond the favourable energy position of ^{3}S* and ^{3}E*, short distances (<1 nm) between the donating and acceptor units are necessary, which might be altered when the solution samples are deposited or prepared in formulations convenient for real devices. In addition, TTET and TTA processes can be inhibited by the presence of O_2 that quenches the triplet excited states.[10]

An important step forward in the application of TTA-UC systems in real devices under air-equilibrated conditions is the

Dipartimento di Chimica, Biologia e Biotecnologie, Università degli studi di Perugia, Via Elce di Sotto 8, Perugia, Italy. E-mail: loredana.latterini@unipg.it

† Electronic supplementary information (ESI) available. See DOI: https://doi.org/10.1039/d2tc00709f

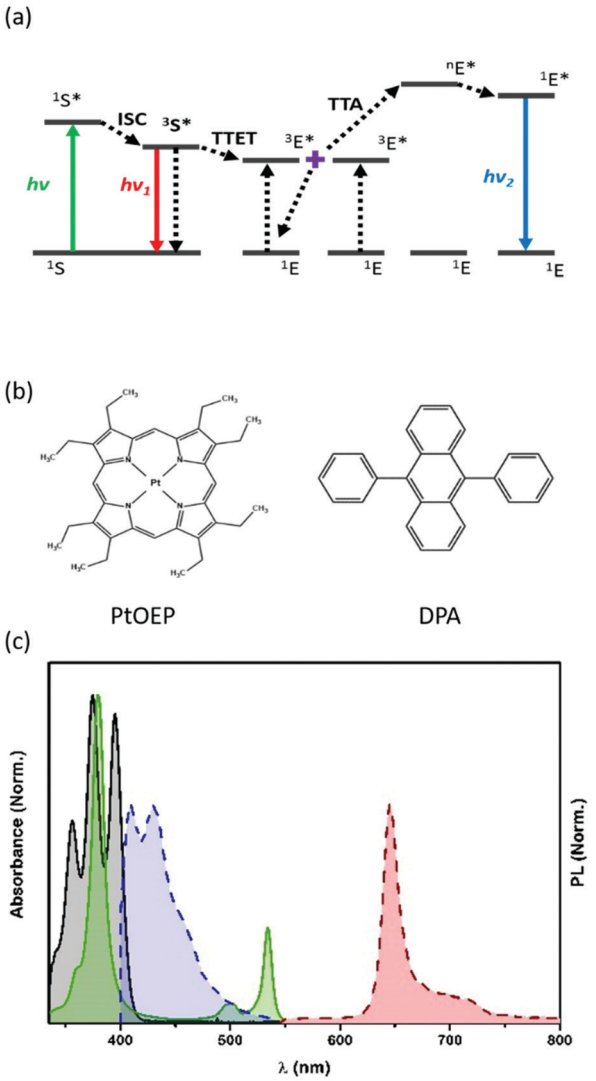

Fig. 1 (a) Scheme of the energy levels involved in the TTA-UC process. (b) Chemical structure of the sensitizer (PtOEP) and emitter (DPA). (c) Absorption and emission spectra of PtOEP (green and red lines, respectively) and DPA (black and blue lines, respectively).

incorporation of the antenna and the emitter pair into protecting environments,[12–15] preserving the inter-chromophoric distances necessary to make efficient bimolecular processes. Therefore, the encapsulation of the organic chromophores presents multiple advantages. Firstly, the nanostructured packaging preserves the possibility of interactions between the sensitizer and the emitter (at TTET distances) and between the emitter molecules to sustain the probability of TTA, independently of medium changes. Secondly, the growth of a silica shell around the dye-doped core, is a promising strategy to compartmentalize the chromophores and create a barrier against oxygen diffusion and protect the chromophores from harsh chemical environments.

A concrete instance of a harsh chemical environment is that originated by the Belousov–Zhabotinsky (BZ) reaction,[16,17] which is an oxidative bromination of malonic acid in the presence of suitable catalysts. The BZ reaction can proceed in the oscillatory regime for many hours in a closed reactor, after a proper choice of the reagent concentrations. These oscillatory conditions have been recently used to prepare biomimetic smart materials[18,19] and perform optical communication experiments.[20–23]

When cerium ions are used as BZ catalysts, they oscillate between the Ce(III) and Ce(IV) states, giving rise to large optical density oscillations in the UV region.[21] UV radiation, with steady intensity and wavelength included in the 300–380 nm range, passing through a solution of the BZ reaction, is transmitted as a modulated UV beam having a period that corresponds to the intrinsic frequency of the BZ reaction (60–80 s). This modulation is due to the different absorption coefficients of the Ce(III) and Ce(IV) ions.[20,24]

However, the chemical environment generated by the BZ reagents is rather aggressive because it is extremely acidic (pH $\approx$ 1) and appreciably oxidative due to the reagent bromate and some intermediates such as bromine and bromous acid, thus making difficult to take full advantage of the optical modulation generated by BZ with "nude" dyes; organic chromophores have very limited stability in the harsh BZ solutions.[20]

Silica capsules have been already proved to fulfil the task of compartmentalizing TTA-UC pairs[4] and preserve the efficiency of the TTA-UC process.

In the present work, we aim to establish the capabilities of the oil-in-silica nanocapsules to protect the benchmark UC-pair (PtOEP and DPA) from the harsh BZ environment and create a barrier against O_2 quenching of the triplet states involved in the TTA-UC process. The up-converting nanocapsules (UC-NC) are efficiently exposed to different irradiation configurations based on incoherent radiation sources (360 or 535 nm and synchronous excitation at 360 and 535 nm) to provide controlled sets of output signals (430 and 645 nm continuous or modulated in intensity).

The achieved results provide a novel proof-of-concept for broadening the relevance and viability of TTA-UC materials in optical communication systems. The results show that the colloidal system made of the UC-NCs and the BZ behaves as an implemented wet-chemical optical multiplexer and demultiplexer.

Results and discussion

Nanocapsule characterization

Oil-in-silica nanocapsules have been prepared following the procedure described in the experimental section and sketched in Scheme S1 (ESI†), obtaining a pinkish powder (inset of Fig. 2(a)). An SEM image of the sample shows spherical nanostructures (Fig. 2(a)), whose morphology and dimensions have been controlled by regulating the synthetic conditions. The analysis of the images enables to determine the diameter distribution of the capsules, which presents the main population centred at 80 nm and a minor one with a mean diameter of about 200 nm (Fig. 2(b)). The red square inset of Fig. 2(a),

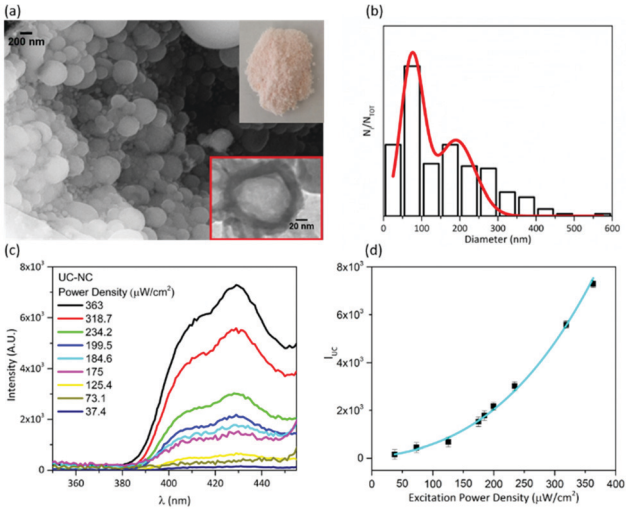

Fig. 2 SEM image of UC-NC ((a) scale bar 200 nm); insets: TEM image (bottom-right, scale bar 20 nm) and photograph (top-right) of the powder; (b) diameter distribution of UC-NC, together with the Gaussian fit; (c) UC emission spectra of solid-state like UC-NC at different power excitation densities at 535 nm; (d) plot of the UC-quantum yield as a function of the excitation power density.

shows a representative TEM image of the sample. The image displays a spherical structure with different contrast; the lighter core is attributed to the oil phase while the darker rim is due to the silica shell whose thickness is about 10–15 nm. These assignments are further supported by FTIR spectra recorded on the powder (Fig. S1, ESI†). The sharp peaks at 2925 cm^{-1} and 2856 cm^{-1} are due to the asymmetric and symmetric CH_2 stretching of oleic acid. The C═O stretching detected at 1714 cm^{-1} indicates the presence of dimeric oleic acid[25] as a result of the compartmentalization inside the silica shell.

The peaks in the 1650–1580 cm^{-1} range can be ascribed to the NH_2 bending in a primary amine like APTES. The peaks at 1080 and 1290 cm^{-1} are assigned to Si–O stretching, and the band at 430 cm^{-1} is due to in-plane bending and out-of-plane rocking of Si–O–Si in a silica network. All these data document the core–shell architecture of the particles. The presence of PtOEP and DPA within the capsules is not evidenced by IR-spectroscopy since their concentration is below the instrumental sensitivity. EDX analysis, carried out on the capsules (Fig. S3, ESI†), does not show the presence of Pt on the silica surface supporting the occurrence of encapsulation of the chromophores.

The information about the absorption features of the nanocapsules is obtained from the UV-Vis reflectance spectrum, once converted in Kubelka–Munk units (Fig. S2, ESI†); the spectrum clearly shows the Soret- and the Q-bands (380 and 510, 535 nm, respectively) of the Pt–porphyrin and the absorption of DPA in the 370–400 nm region.

The up-converted emission from the solid-like samples is recorded upon excitation at 535 nm with a xenon-lamp under air-equilibrated conditions.

The UC-emission of the nanocapsule powder has been monitored as a function of the excitation intensity, and the results are shown in Fig. 2(c). The data are collected using an incoherent excitation source working with a power density between 37.4 μW cm^{-2} and 363 μW cm^{-2}, under air-equilibrated conditions. The results prove the efficiency of SiO_2 shell and oleic acid in making the UC-process air tolerant; in fact, all the measurements are performed without previous deoxygenation. Fig. 2(d) reports the dependence of UC quantum yield on the excitation power density, which shows a quadratic trend. Our results are consistent with the literature data recorded at the low annihilation regime.[26] With the used instrumental setup, a linear regime for the dependence of UC emission on the excitation power was not reached, even after increasing the excitation power up to 363 μW cm^{-2} (maximum accessible). The trend obtained with the UC nanocapsules agrees with the results achieved with another UC pair in toluene solution using a Xe-lamp as the incoherent excitation source.[27] Under the used conditions, the measured UC-quantum yield for the powder samples is 0.01%.

The spectral behavior of UC-emission and the quadratic trend as a function of the excitation power of the solid-state like UC-NC is in accordance with the dependence obtained in oleic acid bulk solution (see Fig. S4, ESI†). In bulk oleic acid solution, an UC-quantum yield value of 0.58% has been measured in an air-equilibrated environment, without previous deoxygenation. For the same UC-couple in hexadecane bulk solutions, the linear regime of the integrated UC emission as a function of excitation power density has been reached in the range of tens of mW cm^{-2}.[28]

The luminescence decays of the chromophores in the nanocapsules have been measured (Fig. 3(a), (c) and (e)) under air-equilibrated conditions. The decays are properly reproduced by multi-exponential functions. Multi-exponential decays are often observed for micro-heterogeneous samples.[29–32] The most correct and accurate method to analyse the data is in terms of decay time distributions, which can be determined using the maximum entropy method. The distribution of the PtOEP phosphorescence decay in the UC-nanocapsules is shown in Fig. 3(b). Two narrow decay populations centred at 1.8 and 6.8 ns, respectively, satisfactorily reproduce the decay profile. The component at 6.8 ns has the largest weight values. The relevant shortening of PtOEP phosphorescence decay times in UC-NC, compared to bulk oleic acid solutions (see Fig. S5, ESI†), suggests that the compartmentalization of the dye molecules inside the capsules, where a more microheterogeneous environment is produced compared to the bulk, might enhance TTET processes or the non-radiative deactivation of the sensitizer. The fluorescence decay time of DPA, when directly excited at 375 nm (Fig. 3(c)) has one dominant decay population centred at 7.8 ns (Fig. 3(d)), whose value is in good agreement with the literature data.[33] The time profile of the up-converted emission (Fig. 3(e)) grows in a time range included between 2 and 4 ns, which is adequately coupled to PtOEP and then decays in a broad range included between 7 and 14 ns (see Fig. 3(f)).

The fuzzy entropy (H, see eqn (2)) is a valuable parameter to quantify the micro-heterogeneity experienced by emitters.[34]

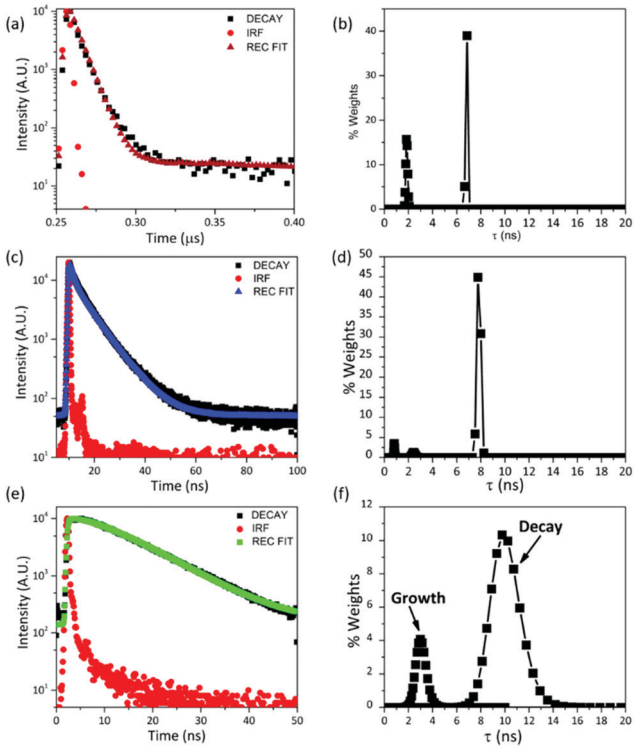

Fig. 3 Emission decay curves recorded from UC-NC powder to detected PtOEP phosphorescence ((a) λ_{exc} = 510 nm and λ_{em} = 645 nm), DPA direct fluorescence ((c) λ_{exc} = 375 nm and λ_{em} = 430 nm) and UC-emission ((e) λ_{exc} = 510 nm and λ_{em} = 430 nm); MEM analysis (b)–(f) of the decays.

The determination of H (see the Experimental section) reveals that PtOEP molecules within the nanocapsules are experiencing a larger micro-heterogeneity degree than that experienced by the sensitizer molecules in bulk oleic acid or toluene solutions (H = 0.27 in nanocapsules, H = 0.21 in oleic acid and H = 0.19 in toluene, see Table 1 and Table S2, Fig. S6 (ESI†) for the MEM distribution). A larger micro-heterogeneity degree is detected for DPA, since H-values are more than doubled going from oleic acid bulk solution (H = 0.11) to the nanocapsules (H = 0.29), but it is worthwhile noticing that the decay distributions of PtOEP and DPA show similar H values when they are embedded in the nanocapsules. The UC-emission presents a more considerable heterogeneity (H = 0.59). The increase of H-values for the UC-emission is likely due to the occurrence of different energy transfer processes from slightly different electronic configurations and/or dispositions, which can be increased in the oil-core of the nanocapsules, as estimated by Monguzzi *et al.*[26] for ordered environments.

Table 1 Luminescence decays of PtOEP, DPA and upconversion in solid-like nanocapsules

λ_{exc} – λ_{em} (nm)	Detected emission	Average decay from MEM distributions	H (fuzzy entropy)
510–645 nm	PtOEP – phosphorescence	τ_1 = 1.8 ns τ_2 = 6.8 ns	0.27
375–430 nm	DPA – fluorescence	τ_1 = 7.8 ns	0.29
510–430 nm	Up-converted emission	τ_1 = 3.0 ns (growth) τ_2 = 10.0 ns	0.59

To further prove the capability of UC-NC to protect the UC-couple, oxygen has been bubbled in the samples and the PtOEP phosphorescence spectra have been collected; PtOEP phosphorescence is a sensitive tool to monitor the occurrence of quenching events. The emission intensity has not been remarkably affected by oxygen in oleic acid and UC-NC, while a substantial quenching has been observed in toluene (Fig. S7, ESI†). This experiment confirms the fundamental role played by the silica shell and oleic acid in preventing the quenching of involved triplet states.

Optical modulation of the emitted radiations

The oxidative bromination of malonic acid catalyzed by cerium ions (Belousov–Zhabotinsky reaction) is a well-known example of oscillatory chemical reaction, which is drawing attention in the field of bio-mimetic materials and neuromorphic engineering.[18–21,35–37] The oscillation of cerium ions, between the two redox states during the BZ reaction, results in a periodic change (with a period of *ca.* 70 s) of the optical density in the 300–380 nm range due to the different absorption coefficients of Ce(IV) and Ce(III) in this spectral region (Fig. S8, ESI†).

The prepared upconverting nanocapsules containing PtOEP and DPA are placed in the cuvette with the BZ reagents and exposed to steady-state radiation at 360 nm. The BZ solution has been prepared to ensure an optical density variation at 360 nm from 0.97 to 0.05 (ΔOD = 0.92), thus modulating the intensity of the residual radiation at 360 nm by about an order of magnitude. Such modulated UV radiation is absorbed by both DPA and PtOEP embedded within the nanocapsules. The chromophores within the nanocapsules, being directly excited, produce two emission signals, one in the blue (centered at 430 nm) due to the fluorescence of DPA, and the other in the red (having a maximum at 645 nm), due to the phosphorescence of PtOEP. Both emissions present modulated intensities as a result of different excitation intensities. The outcome of the above-described modulation experiment is presented in Fig. 4(a) and (b), where the emissions at 430 and 645 nm are monitored for one hour. Both emission signals oscillate with a period in the range of 65–80 s and synchronized in phase with the UV optical density changes determined by the BZ, despite the absence of any physical and chemical interactions between the BZ reaction (acting as transmitter) and PtOEP/DPA in the capsules (receiver). The signals emitted by the luminophores in the receiver capsules are in-phase with the input signal, because the decay time of the emitters (PtOEP and DPA) are quite short (included between the ns and the μs time range) if compared with the period of the oscillations (tuned to be tens of seconds).[38] It is worthwhile noticing that the average intensities of the output signals are constant. This evidence indicates that the silica shell efficiently protects the luminophores from the harsh environment of the BZ reaction for the entire experiment. Thus, we have achieved the goal of guaranteeing the stability of the luminescent compounds in the BZ reaction,

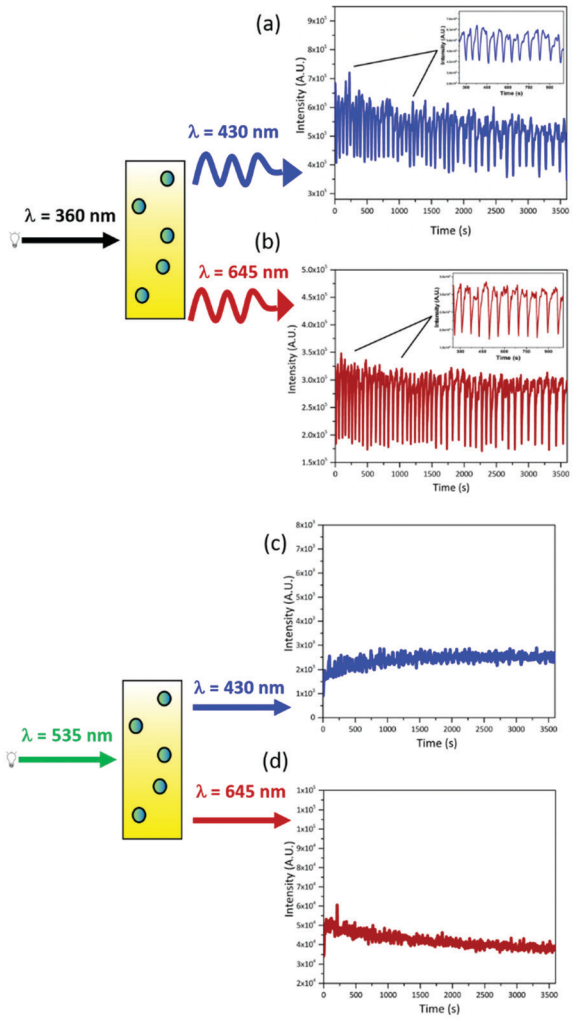

Fig. 4 Schematic diagram of modulation experiment. Output signals of up-converting nanocapsules in BZ-solution (λ_{exc} = 360 nm) recording the emission (a) at 430 nm and (b) at 645 nm. Phosphorescence emission of PtOEP ((d) λ_{exc} = 535 nm, λ_{em} = 645 nm) and upconversion ((c) λ_{exc} = 535 nm, λ_{em} = 430 nm) in nanocapsules dispersed in the BZ solution (power density = 222 μW cm^{-2}).

using silica nanocapsules, compared to the micelles previously used in similar experiments.[20]

The nanocapsules are also capable of generating steady emission signals when excited at 535 nm. In fact, as shown in Fig. 4(c) and (d), when the nanocapsule dispersion is irradiated at 535 nm (far beyond the absorption edge of cerium ions), continuous signals are collected at 645 nm, due to the residual PtOEP phosphorescence, and at 430 nm, ascribable to the TTA-UC process. In this way, we have also demonstrated that the output signal can be tuned from the periodic to the stationary and *vice versa*, by changing the excitation wavelength.

Effect of simultaneous double excitation on the modulation of the emitted radiation

The excitation of UC-NC suspension with the two sources has been further extended to achieve the simultaneous exposure of the capsules to the modulated 360 nm and to the steady state 535 nm radiations. The emission is monitored at 430 nm and 645 nm (Fig. 5), to evaluate the impact of the concomitant excitations on up-converted and linear emissions and the possibility of extending the optical output from the chemical sample.

We have already shown that the exposure of DPA to the periodic 360 nm results in a periodic emission at 430 nm due to the direct excitation of the annihilator molecules. Upon adding steady-state 535 nm excitation, the fluorescence loses amplitude but preserves the periodic behaviour (Fig. 5(a)). The radiation at 535 nm originates triplet states of PtOEP that transfer their energy to DPA molecules, producing triplet states of DPA. Hence, the number of DPA molecules in their electronic ground state, which can absorb the 360 nm radiation, is reduced (it has to be noted that under the used experimental conditions, DPA absorbs about 30–35% of 360 nm radiation). This depletion of DPA molecules, in their ground state due to the excitation at 535 nm, is responsible for the reduction of the oscillation amplitudes. The larger the shrinkage of the oscillation amplitudes, the more significant is the DPA depletion. The maximum amplitude reduction is observed when the power density at 360 nm is 1 μW cm^{-2}, upon additional exposure to 535 nm light (about 38%, Fig. 5(a)); using higher power densities at 360 results in a lower or negligible depletion of DPA molecules when 535 nm radiation is turned on (Table 2 and see also Fig. S9, ESI†), indicating that the UC-process is competitive with direct excitation only at low UV-densities.

The power densities have been used to estimate the number of 360 nm or 535 nm photons involved in the experiments. Selecting 1 μW cm^{-2} at 360 nm corresponds to exposing the sample to *ca.* 2 × 10^{12} photons s^{-1} cm^{-2}, 33% of which are

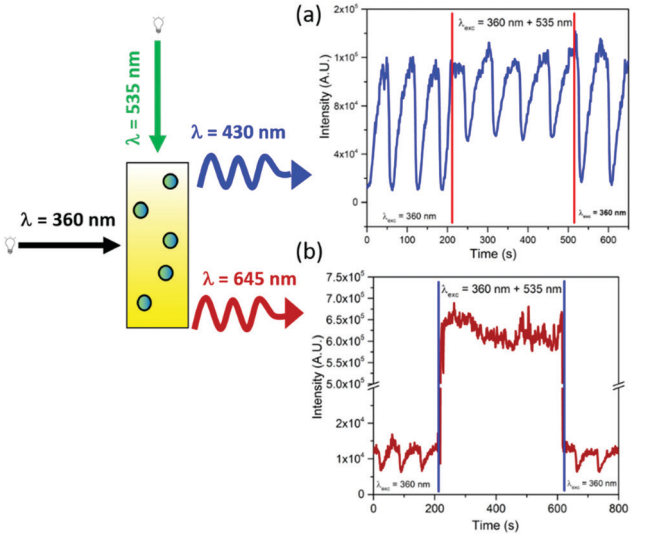

Fig. 5 Schematic diagram of the modulation experiment with double excitation. (a) Output signals at 430 nm upon excitation at 360 nm (1 μW cm^{-2}, for the entire experiments) plus excitation at 535 nm (55 μW cm^{-2}) at times indicated by the blue lines. (b) Output signal at 645 nm upon excitation at 360 nm (133 μW cm^{-2}) plus excitation at 535 nm (55 μW cm^{-2}).

Table 2 Reduced amplitude of the output signal of emission at 430 nm due to UC-emission calculated according to the procedure shown in Scheme S2 (ESI)

Power density at 360 nm (μW cm^{-2})	Δ-Amplitude (%)
13	18
6	19
1	38

absorbed by DPA (considering the fraction of light absorbed by DPA, based on its and PtOEP absorbances at 360 nm) and essentially converted into direct fluorescence. On the other hand, using 55 μW cm^{-2} at 535 nm results in irradiating the sample with *ca.* 2×10^{14} photons s^{-1} cm^{-2}, all absorbed by PtOEP; considering an UC-quantum yield of the UC-NC of 0.01%, *ca.* 5×10^{9} photons s^{-1} cm^{-2} are expected to be up-converted. These valuations would suggest that under the used experimental conditions, steady-state up-conversion should compete with direct DPA fluorescence, while it is not experimentally observed.

The phosphorescence of the sensitizer molecules, at 645 nm, has a periodic behaviour when PtOEP is exposed to periodic 360 nm radiation; the periodicity is determined by the oscillating concentration of the PtOEP triplet state generated by the periodic intensity of the 360 nm radiation. However, with the addition of steady excitation at 535 nm, the phosphorescence gains almost two orders of magnitude in intensity and loses its periodic trend (Fig. 5(b)). These observations suggest that PtOEP emission is dominated by the steady-state excitation; indeed, reducing the intensity of the 535 nm radiation, inserting neutral density filter, the oscillations caused by the synchronization of PtOEP excited state with the BZ period are observable (see Fig. S10, ESI†).

These data, together with the analysis of the emission time-resolved profiles of the capsules (see above), indicate that despite the important protecting action of the oil-in-silica structures, the compartmentalization of the dyes enhance non-radiative deactivation path of the dyes limiting the UC-efficiency.

However, the presented results evidence that TTA-UC capsules, prepared to control the concentration of sensitizers and emitting units, are a valuable and flexible system in the development of materials and read-out procedures for the application in the optical communication field.

Experimental

Materials

2,3,7,8,12,13,17,18-Octaethyl-21*H*,23*H*-porphyrin platinum(II) (PtOEP), 9-10-diphenylanthracene (DPA), tetrahydrofuran (THF), oleic acid, tetraethyl orthosilicate (TEOS), 3-aminopropyltriethoxysilane (APTES), perylene, malonic acid, $NaBrO_3$, H_2SO_4, $Ce(SO_4)_2$ and ethanol were purchased from Sigma-Aldrich. Deionized water was obtained by a reverse osmosis process on a Milli-Q system (Millipore, Rome, Italy). All reagents and solvents were used as received without further treatment.

Synthesis of nanocapsules

The synthesis of oil core/silica shell nanocapsules is carried out through the microemulsion method, following the method reported by Kwon *et al.*[4] with some modifications. The process occurs in two steps (Scheme S1, ESI†); first, a stock solution of PtOEP and DPA in THF (that acts as co-solvent) is prepared with a concentration of 20 mM and stored under dark conditions. Then, 125 μL of PtOEP (0.5 mM) and 300 μL of DPA (1.2 mM) are added to 5 mL of oleic acid; the solution is kept at 70 °C overnight to completely remove THF.

300 μL of solution are added to 28.8 mL of deionized water to create the microemulsion. Afterwards, the microemulsion is stirred at room temperature for 1 h. 234 μL of APTES were dripped slowly and then, 2 mL of TEOS were rapidly added. The microemulsion was left at room temperature for 1 hour, and then was maintained at 50 °C under magnetic stirring for 24 h. The powder was recovered by washing/centrifuge cycles. The nanocapsules were dried at 60 °C.

Morphological and structural characterization

Transmittance electron microscopy (TEM) images are collected on a Philips model 208 microscope operating at 80 kV of beam acceleration. The morphology of the samples is also investigated on an FEG LEO 1525 scanning electron microscope (SEM). FE-SEM micrographs are collected after depositing the powder samples on the stub and sputter coated with chromium for 8 seconds to have a Cr-layer of 20 nm. Analysis of SEM images enables obtaining the diameter distribution of the nanocapsules, which is statistically examined. The elemental composition and chemical mapping are determined through Energy Dispersive X-ray Analysis (EDX), using a Bruker Quantax EDS.

ATR-IR spectra in the 4000–400 cm^{-1} frequency range are recorded on an ALPHA compact FT-IR BRUKER, equipped with a diamond crystal; each spectrum is the average of 30 scans with a 2 cm^{-1} resolution.

Optical characterization

Reflectance spectra of the powder samples are recorded on a Varian (Cary 4000) spectrophotometer, equipped with a 150 nm integrating sphere (DRA-900). The collected spectra are then converted into Kubelka–Munk units.[39] UV-Visible spectra of the suspensions are collected on a Cary 8454 Diode Array spectrophotometer in a quartz cuvette with an optical path of 1 cm. The photoluminescence spectra of the samples are measured using the fluorospectrophotometer Fluorolog (Spex F112AI) equipped with a 450 W xenon lamp. The emission spectra of the powders are measured using a front-face geometry. The recorded up-conversion emission spectra are corrected according to the method described proposed by Kubista.[39] The up-conversion quantum yield has been estimated according to the

following eqn (1):

$$\Phi_{UC} = \Phi_{STD} \times \frac{Abs_{STD}}{Abs_S} \times \frac{I_S}{I_{STD}} \times \left(\frac{\eta_S}{\eta_{STD}}\right)^2 \quad (1)$$

where Φ_{STD} is the fluorescence quantum yield of the standard (Rhodamine 6G, 0.94 in ethanol), Abs_S and Abs_{STD} are the absorbance at the excitation wavelength of the UC sample and the Rhodamine 6G, respectively. It has to be noted that in the case of the capsule sample, Abs_S accounts for scattering, I_S and I_{STD} represent the integrated emission intensity of the UC solution and the standard respectively while η are the refractive indices of ethanol (with subscript STD) and oleic acid (with subscript S). The excitation power density is measured using a radiometer Avaspec-ULS2048CL-EVO.

Emission decay profiles are collected through the spectrofluorometer Edinburgh FS5; the up-conversion kinetic profile and phosphorescence decay of PtOEP are collected using a diode centred at 510 nm as the excitation source and monitoring the luminescence at 430 nm and 645 nm, respectively.

For comparison, fluorescence decays of DPA in the UC-sample are also recorded upon direct DPA excitation at 375 nm. The emission decay profiles, $I(t)$, are analysed through both the nonlinear least-squares method and the Maximum Entropy Method (MEM) through the MemExp Software.[40,41]

The micro-heterogeneity of the samples has been evaluated by determining the fuzzy entropy (H),[42,43] defined according to eqn (2):

$$H = -\frac{1}{\log(N)} \sum_{i=1}^{N} (w_i \log(w_i)) \quad (2)$$

In eqn (2), N is the number of exponential terms of the poly-exponential fitting function $I(t) = \sum_{i=1}^{N} A_i e^{-t/\tau_i} I$ whereas $w_i = A_i \Big/ \left(\sum_{i=1}^{N} A_i\right)$ is the weight of the i-th exponential term. The fuzzy entropy H is normalized and can assume values included between 0 and 1. The more heterogeneous the luminophore environment, the larger the H-value.[34]

Emission modulation experiments

The BZ reaction was performed by adding malonic acid (0.3 M in water), $NaBrO_3$ (0.088 M) dissolved in H_2SO_4 0.875 M and $Ce(SO_4)_2 \cdot nH_2O$ (0.0045 M) in H_2SO_4 1 M, in a cuvette with 1 cm path length. Then, the upconverting nanocapsules (4 mg mL^{-1}) were added. Upon excitation at 360 nm, luminescence was collected at 430 nm and 645 nm, corresponding to the maxima DPA and PtOEP emissions, respectively. Both signals are acquired for 1 h, keeping the sample under vigorous magnetic stirring. The time-base acquisition was recorded by a Fluorolog (Spex F112AI) spectrofluorometer using a xenon lamp with an excitation power at 360 nm included between 100 μW cm^{-2} and 133 μW cm^{-2}.

For the experiments with double excitation, a second xenon lamp equipped with a band-pass filter centred at 535 ± 15 nm was employed in addition to the source at 360 nm (133 μW cm^{-2}), to excite PtOEP selectively. The excitation at 360 nm was maintained for the entire experiment, while the radiation at 535 nm was applied to the sample at specified time intervals; the optical modulation of the radiation was monitored for 1800 s.

The output signals at 430 and 645 nm were registered; the power density of 360 nm and 535 nm were selectively varied between 13–1 μW cm^{-2} and 55–2.8 μW cm^{-2}, respectively.

Conclusions

In this work, oil in silica up-converting nanocapsules have been synthesized, and the up-conversion emission based on triplet–triplet annihilation of the benchmark couple composed of PtOEP/DPA is studied in solid-state like and suspensions. The up-converted emission has been detected in the solid-state like in an air-equilibrated environment, using an incoherent low power excitation source. Thus, the silica shell slows down the oxygen diffusion inside the capsules. Moreover, the core of oleic acid reacts with the oxygen species, avoiding the quenching of the porphyrins' triplet excited state. In order to further test the robustness of the nanostructured packaging, the up-converting capsules have been used in the harsh aqueous solution of the Belousov–Zhabotinsky (BZ) reaction; this oscillatory chemical system acts as a transmitter of a periodic signal and the photo-excitable compounds inside the nanocapsules behave as receivers. Even if the transmitter and the receivers are in the same cuvette, the chromophores are protected from the chemical environment generated by the BZ, thanks to the thick silica shell nanocapsules. The advantages of the implemented device are many: the optical response in a periodic regime occurs at two different wavelengths (430 nm and 645 nm) using the same excitation energy (360 nm). Moreover, the emission of the receiver is modulated in a continuous or oscillatory regime, depending on the excitation wavelength. The experiments with double excitation show that the signal at 645 nm can be switched from periodic to continuous when the system is irradiated at 535 nm with sufficiently powerful radiation in the stationary regime.

In conclusion, the present work represents an interesting way of developing nanostructured chemical systems for the modulation of the radiation in the periodic regime across the visible spectrum and provides a proof-of concept for the demultiplexer behaviour of the investigated system.

Author contributions

Conceptualization L. L., P. L. G.; data curation P. L. G., G. Q.; formal analysis P. L. G., G. Q.; investigation G. Q., B. B.; methodology L. L.; supervision L. L., P. L. G.; validation P. L. G., G. Q.; writing – original draft L. L., G. Q.; writing – review & editing G. Q., B. B., P. L. G., L. L.

Conflicts of interest

There are no conflicts to declare.

Acknowledgements

We thank Prof. Paola Sassi and Prof. Marco Paolantoni for their support with ATR-IR measurements. The Università degli Studi di Perugia and the Ministero per l'Università e la Ricerca Scientifica (MIUR – Rome) are acknowledged for support through the program "Dipartimenti di Eccellenza 2018–2022" (grant AMIS). L. L. is grateful to CSGI (Consorzio Interuniversitario per lo Sviluppo dei Sistemi a Grande Interfase, Research Center for Colloid and Surface Science) for the scientific support.

References

1 T. A. Lin, C. F. Perkinson and M. A. Baldo, *Adv. Mater.*, 2020, **32**, 1908175.
2 A. Ansari, V. K. Thakur and G. Chen, *Coord. Chem. Rev.*, 2021, **436**, 213821.
3 Y. Gao, S. Murai, K. Shinozaki, S. Ishii and K. Tanaka, *Adv. Opt. Mater.*, 2021, **9**, 2001040.
4 O. S. Kwon, H. S. Song, J. Conde, H. I. Kim, N. Artzi and J. H. Kim, *ACS Nano*, 2016, **10**, 1512–1521.
5 E. M. Gholizadeh, S. K.-K. Prasad, Z. L. Teh, T. Ishwara, S. Norman, A. J. Petty, J. H. Cole, S. Cheong, R. D. Tilley, J. E. Anthony, S. Huang and T. W. Schmidt, *Nat. Photonics*, 2020, **14**, 585–590.
6 Y. Zhou, F. N. Castellano, T. W. Schmidt and K. Hanson, *ACS Energy Lett.*, 2020, **5**, 2322–2326.
7 T. F. Schulze and T. W. Schmidt, *Energy Environ. Sci.*, 2015, **8**, 103–125.
8 T. N. Singh-Rachford and F. N. Castellano, *Coord. Chem. Rev.*, 2010, **254**, 2560–2573.
9 X. Zhu, Q. Su, W. Feng and F. Li, *Chem. Soc. Rev.*, 2017, **46**, 1025–1039.
10 V. Gray, *Photochemistry*, 2019, **47**, 404–420.
11 Y. V. Aulin, M. Van Sebille, M. Moes and F. C. Grozema, *RSC Adv.*, 2015, **5**, 107896.
12 V. Gray, K. Moth-Poulsen, B. Albinsson and M. Abrahamsson, *Coord. Chem. Rev.*, 2018, **362**, 54–71.
13 L. Latterini, G. Massaro, M. Penconi, P. L. Gentili, C. Roscini and F. Ortica, *Dalton Trans.*, 2018, **47**, 8557–8565.
14 D. F. Barbosa de Mattos, A. Dreos, M. D. Johnstone, A. Runemark, C. Sauvée, V. Gray, K. Moth-Poulsen, H. Sundén and M. Abrahamsson, *J. Chem. Phys.*, 2020, **153**, 214705.
15 S. N. Sanders, M. K. Gangishetty, M. Y. Sfeir and D. N. Congreve, *J. Am. Chem. Soc.*, 2019, **141**, 9180–9184.
16 R. Epstein and J. A. Pojman, *An introduction to nonlinear chemical dynamics: oscillations, waves, patterns, and chaos*, Oxford University Press, NY, 1998.
17 R. J. Field, E. Koros and R. M. Noyes, *J. Am. Chem. Soc.*, 1972, **94**, 8649–8664.
18 K. Inui, I. Saito, R. Yoshida, H. Minato and D. Suzuki, *ACS Appl. Polym. Mater.*, 2021, **3**, 3298–3306.
19 T. Geher-Herczegh, Z. Wang, T. Masuda, R. Yoshida, N. Vasudevan and Y. Hayashi, *Macromolecules*, 2021, **54**, 6430–6439.
20 P. L. Gentili, M. S. Giubila, R. Germani, A. Romani, A. Nicoziani, A. Spalletti and B. M. Heron, *Angew. Chem., Int. Ed.*, 2017, **56**, 7535.
21 P. L. Gentili, M. S. Giubila, R. Germani and B. M. Heron, *Dyes Pigm.*, 2018, **156**, 149–159.
22 A. Walther, *Adv. Mater.*, 2020, **32**, 1905111.
23 G. Cheng, C. Lin and J. Pérez-Mercader, *Small*, 2021, **17**, 2101162.
24 P. L. Gentili and J. C. Micheau, *J. Photochem. Photobiol., C*, 2020, **43**, 100321.
25 G. Blyholder, C. Adhikar and A. Proctor, *Colloids Surf., A*, 1995, **105**, 151–158.
26 A. Monguzzi, J. Mezyk, F. Scotognella, R. Tubino and F. Meinardi, *Phys. Rev. B: Condens. Matter Mater. Phys.*, 2008, **78**, 195112; Y. Y. Cheng, T. Khoury, R. G.-C. R. Clady, M. J.-Y. Tayebjee, N. J. Ekins-Daukes, M. J. Crossleya and T. W. Schmidt, *Phys. Chem. Chem. Phys.*, 2010, **12**, 66–71; A. Haefele, J. Blumhoff, R. S. Khnayzer and F. N. Castellano, *J. Phys. Chem. Lett.*, 2012, **3**(3), 299–303.
27 M. Penconi, F. Ortica, F. Elisei and P. L. Gentili, *J. Lumin.*, 2013, **135**, 265–270.
28 G. Massaro, J. Hernando, D. Ruiz-Molina, C. Roscini and L. Latterini, *Chem. Mater.*, 2016, **28**, 738–745.
29 C. Bellacanzone, L. Tarpani, P. L. Gentili and L. Latterini, *J. Lumin.*, 2020, **226**, 117513.
30 G. Massaro, P. L. Gentili, V. Ambrogi, M. Nocchetti, F. Marmottini, F. Ortica and L. Latterini, *Microporous Mesoporous Mater.*, 2017, **246**, 120.
31 P. L. Gentili, C. Clementi and A. Romani, *Appl. Spectrosc.*, 2010, **64**, 923–929.
32 P. L. Gentili, *Dyes Pigm.*, 2014, **110**, 235–248.
33 M. Montalti, A. Credi, L. Prodi and M. T. Gandolfi, *Handbook of photochemistry*, CRC Press, 2006.
34 P. L. Gentili, *Molecules*, 2018, **23**, 2074.
35 S. Proskurkin, P. S. Smelov and V. K. Vanag, *Phys. Chem. Chem. Phys.*, 2020, **22**, 19359–19367.
36 G. Gruenert, K. Gizynski, G. Escuela, B. Ibrahim, J. Gorecki and P. Dittrich, *Int. J. Neural Syst.*, 2015, **25**, 1450032.
37 T. Litschel, M. M. Norton, V. Tserunyan and S. Fraden, *Lab Chip*, 2018, **18**, 714–722.
38 M. S. Chern, N. Watanabe, K. Suga, Y. Okamoto and H. Umakoshi, *Langmuir*, 2021, **37**, 6811–6818.
39 M. Kubista, R. Sjöback, S. Eriksson and B. Albinsson, *Analyst*, 1994, **119**, 417–419.
40 P. J. Steinbach, R. Ionescu and C. R. Matthews, *Biophys. J.*, 2002, **82**, 2244–2255.
41 P. J. Steinbach, *J. Chem. Inf. Comput. Sci.*, 2002, **42**, 1476–1478.
42 B. Kosko, *Inform. Sci.*, 1986, **40**, 165–174.
43 P. L. Gentili, *Molecules*, 2021, **26**, 5987.

